Annals of Mathematical Sciences and Applications
Volume 1, Number 1, 149–180, 2016

# Large eddy simulation, turbulent transport and the renormalization group

James Glimm, Bradley J. Plohr, Hyunkyung Lim,
Wenlin Hu, and David H. Sharp

In large eddy simulations, the Reynolds averages of nonlinear terms are not directly computable in terms of the resolved variables and require a closure hypothesis or model, known as a subgrid scale term. Inspired by the renormalization group (RNG), we introduce an expansion for the unclosed terms, carried out explicitly to all orders. In leading order, this expansion defines subgrid scale unclosed terms, which we relate to the dynamic subgrid scale closure models. The expansion, which generalizes the Leonard stress for closure analysis, suggests a systematic higher order determination of the model coefficients.

The RNG point of view sheds light on the numerical nonuniqueness of the infinite Reynolds number limit. For the mixing of $N$ species, we see an $N + 1$ parameter family of infinite Reynolds number solutions labeled by dimensionless parameters of the limiting Euler equations, in a manner intrinsic to the RNG itself. Large eddy simulations, with their Leonard stress and dynamic subgrid models, break this nonuniqueness and predict unique model coefficients on the basis of theory. In this sense, large eddy simulations go beyond the RNG methodology, which does not in general predict model coefficients.

AMS 2000 subject classifications: 76F65, 76F35, 82B28.
Keywords and phrases: LES, renormalization group, subgrid scale models.

## 1. Introduction

Turbulence is one of the major unsolved problems of classical physics, a view attributed to Heisenberg, among others. Turbulence is an instability of fluid flow which occurs at high Reynolds numbers $\mathrm{Re} = VL/\nu$, where $V$ and $L$ are representative velocities and lengths and $\nu$ is the kinematic anisotropic viscosity. Many turbulent flows, including ones arising in oceanography, atmospheric sciences, aeronautics, astrophysics and chemical processing occur at elevated, nearly infinite Reynolds numbers.

Turbulence is a strong coupling theory with no natural length scales internal to the turbulently active (inertial) range of scales. For this reason numerical solutions of turbulent flow, when cut off at some grid level within the inertial range encounter difficulties in the coupling between the resolved (grid level) data and the unresolved (subgrid level) data. Because of the strong coupling, scale invariant nature of subgrid scale turbulence, methods to treat this effect on the resolved scales have been introduced. Large Eddy Simulation (LES) is such a numerical method in which some, but not all, of the turbulent scales are resolved, and subgrid scale models emulate the influence of the unresolved on the resolved scales.

The strong coupling problem originates in the nonlinearity of the compressible Navier-Stokes equations, which govern the turbulent flow field. The averaging operation used to define grid level quantities suitable for numerical computation, when applied to nonlinear terms in the Navier-Stokes equations, leads to new unknown flow quantities, called subgrid scale (SGS) terms. Supplying approximations to the SGS terms is a process known as *closure*. The averaged nonlinear terms, before approximation, are called unclosed.

Standard LES/SGS methods address what might be called the cannonical nonlinearities of the Navier-Stokes and related continuum physics equations, namely those related to turbulent viscosity, thermal conductoin and species diffusion. These are all quadratic in the primitive equation variables, and are subsumed within the RNG framework developed here. Missing from this analysis, and often a central difficulty for computational continuum physics, is a methodology to address subcell variation and averages of nonquadratic nonlinear terms in the governing equations. These are often thermodynamically dependent, such as pressure, chemical reaction rates, material strength, opacity, and molecular level viscosity, thermal conduction and species diffusion. Front Tracking, with its possibility of subcell or cut cell resolution, offers a partial solution for such problems.

The major themes of this paper are: nonuniqueness for numerical solutions of a dynamic evolution problem, appropriate usage of SGS terms, their selection, if to be used, the role of the RNG as framework for understanding the selection of SGS terms, the need for Front Tracking to address or mitigate difficulties associated with nonlinearities out of the scope of LES/SGS, and the verification and validation (V&V) of a specific recipe (FT/LES/SGS). i.e., dynamic SGS and front tracking both to limit numerical diffusion and to control mixed cell flow parameters beyond the scope of SGS terms.

We list four new results of our presentation. The first main result concerns numerical nonuniqueness of LES, Sec. 2.1. The second is a reworking of

the RNG formalism, in a manner adapted to the needs of LES, see Secs. 2.2, 2.3. Details of this analysis are presented in Secs. 3 and 4. The connection of RNG to the choice of SGS model coefficients is given in Sec. 5. A first (to our knowledge) analysis of cubic nonlinearities is given in Sec. 6.2, as a third result. As far as we are aware, there is no systematic and theoretically based methodology for closure of triple correlations, even in leading order; the present analysis sheds some light on this issue. It appears that the cubic terms would be naturally defined in a second order LES closure framework, in which quadratic quantities become dynamic (primitive) variables, with their own evolution equations. Such second order closures are not normally considered in an LES framework, but are common in a RANS framework.

Our fourth main result, presented in Sec. 7, is to explore the role of numerical issues in modifying or selecting the RNG limit point. New simulation results with comparison to experiment and to nearly DNS simulations are included. Evidence of numerical nonuniqueness of solutions is presented. A concluding discussion is found in Sec. 8.

Relevant to the present work, we mention our own studies of turbulent mixing [20, 22, 14, 27]. We also mention our related K41 based existence theorem for $L^p$ solutions of the incompressible constant density Euler equations [2].

## 2. RNG applied to LES

In the limit $\mathrm{Re} \to \infty$, the theory simplifies and scaling laws apply, the most famous of which is that of Kolmogorov [17]. The renormalization group (RNG) is a method for the systematic study of scaling laws. The RNG framework is explained in [26], with the goal of finding an expression for the unclosed terms in a LES mentioned.

RNG applied to turbulence has been developed as a systematic body of work [41, 42, 40]. This work is applied to single fluid incompressible turbulence, with all problem specific information removed by scaling transformations. The resulting equations are analyzed in Fourier space, and approximations are evaluated via the epsilon expansion, leading to values for a number of universal parameters which characterize turbulence in agreement with experiment and simulation, including the Kolmogorov constant and turbulent Prandtl number.

This body of work is not yet sufficient for the needs of many engineering and scientific studies, for several reasons. Often such problems are compressible and multifluid, with the multiple fluids fully coupled and not passive scalars. Often problem specific details cannot and should not be removed

and continue to interact with turbulent quantities, Most practical simulations rely on Reynolds Averaged Navier-Stokes (RANS) simulations. These require settings of multiple parameters, from experiment, LES or Direct Numerical Simulation (DNS) or theory. However, the parameters are observed in practice to be nonuniversal and problem dependent, so that the universal parameters from RNG, even when matching the parametric needs of RANS, can offer only general guidance and not problem specific parameter settings. Finally for use with LES, where the turbulent flow is partially simulated, the residual parameters, such as turbulent viscosity are needed not in a universal form but as a residual quantity, applicable to subgrid flows below a certain grid level.

For these reasons, we recast the RNG approach in a manner better suited to the needs of LES. We operate in position space, we omit the epsilon expansion, we rely on LES specific methods to evaluate approximations and we omit the rescaling typical of RNG studies. With these modifications, we still use an RNG coarse graining expansion but do not seek an RNG fixed point.

The study of SGS terms is central to this paper. Each closed SGS approximation term is regarded as a product of a coefficient and a solution functional of specified form. We call the latter a model. The method of dynamic SGS terms uniquely specifies the coefficient once the model is given. This determination is based on properties of the resolved scales, connected to analogous properties of the unresolved scales by an asymptotic assumption. We motivate this derivation by RNG concepts, Thus the coefficient is determined by theory, leaving the model selection open as a subject for research. The search for alternate frameworks for the choice of SGS terms is an active topic of research, which we do not attempt to review here, but we do discuss problems which arise if the SGS models are omitted completely, as commonly occurs when the Implicit Large Eddy Simulation (ILES) method is used.

We derive a closed form expansion for the unclosed terms in the Reynolds averaged equations, founded on RNG ideas, with (for a finite expansion) a closed form remainder. RNG methods, by themselves, do not predict the equation coefficients, so that dynamic LES methods, which do, are an extension of the RNG methodology. At leading order, this expansion is a step in the derivation of closures for the quadratic SGS terms, coinciding with the derivation of the Leonard stress. The leading order term of our expansion is related to the Clark model [3]. Due to stability problems with the Clark model, which arise because the exact SGS terms are not definite, the exact closures, even in leading order, are further approximated, most commonly by gradient diffusion models in a Smagorinsky tradition.

### 2.1. Nonuniqueness of numerical solutions

The first main contribution in this paper, of a speculative nature, consists of observations concerning the nonuniqueness of the Re $\to \infty$ limit, a phenomenon that is naturally understood within the RNG framework. We identify numerical nonuniqueness as an issue for verification methodology.

Nonuniqueness is an issue for the (still used) ILES method, in which explicit SGS terms are replaced by algorithmic details, resulting in nonunique (effective, numerically or algorithmically driven) SGS terms and nonuniqueness of the solution. Nonuniqueness is also an issue for DNS or nearly DNS simulations, as we examine in more detail in Sec 7. DNS, by definition, is the resolution of all relevant length scales. Missing is a systematic procedure to assure which scales must be resolved. The answer surely depends on the observable being computed and the required accuracy for the computation, so a comparison to some turbulence related length scale, sufficient for some questions, may require a more stringent comparison for others. It is evident that DNS has its own need for verification and validation, just as does the rest of science. Nonuniqueness is related to thermal or concentration diffusion mixing, according to a picture we sketch below, but it is also associated with mixed cell thermodynamics, a topic out of the scope of SGS terms, see Sec. 2.4.

In the RNG line of reasoning, the Euler equations, as a limit of the Navier-Stokes equations, arise as an RNG fixed point. We have postulated [22, 14] that for the mixing of $N$ species, the high Re limit point is not unique; rather, it is chosen from an $N+1$ parameter family of limit points, labeled by points $T \in \mathcal{T}$, with $\mathcal{T}$ being the $(N+1)$-dimensional space of transport coefficient ratios for the Navier-Stokes equation, namely the $N-1$ independent dimensionless mass diffusivities (Schmidt numbers), the dimensionless thermal diffusivity (the Prandtl number), and the dimensionless ratio of the anisotropic and isotropic viscosities. In the case of multi-temperature thermodynamics, $\mathcal{T}$ is $2N$ dimensional, the increase resulting from $N-1$ new Prandtl numbers. Each sequence Re $\to \infty$ is accompanied by a sequence $T(\mathrm{Re}) \in \mathcal{T}$, which we assume to be convergent: $T(\mathrm{Re}) \to T(\mathrm{Re} = \infty)$. Dimensional transport coefficients are denoted as $t$. In the limit Re $\to \infty$ as we define it, $t \to 0$, but other choices of the limit Re $\to \infty$ are possible, as we illustrate below. Further comments on nonuniqueness are given in Sec. 8.

As a simple illustration of the nonuniqueness of the RNG limit, consider two different physically motivated pictures. In case A, as a model of turbulent combustion, the thermal diffusion is molecular in nature and en-

hanced by turbulent mixing. For this limit, we keep fixed the dimensionless Prandtl number $\mathrm{Pr} = \nu/\kappa$, where $\kappa$ is the thermal diffusivity and $\nu$ is the kinematic anisotropic viscosity, to preserve the dimensionless aspects of the thermal mixing processes; the other dimensionless transport coefficients are also fixed in the same manner. In case B, we assume a thermal process unrelated to turbulent mixing (such as radiation), for which we want to keep $\kappa$ constant so that $\mathrm{Pr} \to 0$ as $\mathrm{Re} \to \infty$. The limiting equations in the two cases A and B do not coincide. For case A, the limiting equations are the Euler equations, with all transport coefficients set to zero, and for case B, the limiting equations include a thermal diffusion term in the energy equation.

The full $N + 1$ parameter space of RNG limit points is realized by alternate paths in $\mathcal{T}$, taken as $\mathrm{Re} \to \infty$. Alternate paths may originate from alternate choices for the subgrid scale models, or from alternate physical modeling, leading to alternate settings of the laminar transport coefficients $t(\mathrm{Re})$, as indicated above (cases A and B).

Related to this physics-level nonuniqueness is a numerical nonuniqueness. Different numerical algorithms applied to an identical problem yield apparently converged solutions with significant qualitative differences [4, 25, 27]. The SGS terms which select among the $N + 1$ parameter family of solutions are commonly omitted in an ILES framework, or treated implicitly as an aspect of the algorithm itself. Moreover, whether the differencing is ILES or LES with subgrid terms, the numerical truncation errors contribute at a comparable order and also participate in the selection of the limit from among the $N + 1$ parameter family of possible solutions. For this reason, we propose Front Tracking to limit the numerical contributions to the transport coefficients.

As a side note, we observe that nonuniqueness has been demonstrated mathematically for some time [37].

### 2.2. Three RNG steps

The RNG has three basic operations:

1. an integration or coarse-graining step, which partially solves the equation in mapping the unknown solution from a fine to a coarser grid;
2. a remapping or rescaling step, which changes the length scales so that the unknown length scale of the coarser grid is always fixed;
3. a re-parameterization step, in which certain solution parameters (the coefficients of the "relevant" terms) are assigned new, or updated, values to assure continued agreement with parameters that define the

observed solutions. This agreement is obtained from measurements at the length scale of the coarse grid.

We propose to label the relevant variables by the $N + 1$ parameters of $\mathcal{T}$; see additional discussion in Sec. 8. For each parameter of $\mathcal{T}$, we need an observable, defined on the coarse grid, to determine that parameter. To establish a bridge to the LES terminology, we call these observables *models*.

We apply the RNG construction to estimate subgrid scale terms associated with a grid $\mathcal{M}_n$. On this grid some terms (namely, the averages of the nonlinear terms in the Navier-Stokes equations) are unresolved, in the sense that they fail to be functions only of the averaged primitive variables. The averaged primitive variables are constant on each cell of the grid $\mathcal{M}_n$.

The RNG step 1 is an integration, i.e., a coarse graining step. This map of solutions induces a map of equations, namely the equations satisfied by the mesh averages of the solutions. The map of equations is straightforward as far as linear equation terms are concerned. (See Secs. 3 and 4.) But the map leads to unresolved (unclosed) terms when applied to nonlinear terms in the equation. These unclosed (as far as $\mathcal{M}_n$ is concerned) terms are identified as polynomials in first difference operators defined on $\mathcal{M}_{n+1}$. We iterate on step 1, with step 2 removed. In this way, we start the coarse graining, in successive RNG iterations, from $\mathcal{M}_{n+2}, \cdots, \mathcal{M}_{n+k}, \cdots$. This construction of unclosed terms for equations on $\mathcal{M}_n$ yields a product of polynomials in first difference operators on each of $\mathcal{M}_{n+1}, \cdots, \mathcal{M}_{n+k}, \cdots$.

In this mapping the SGS terms, the expressions unresolved at some mesh level $\mathcal{M}_n$ are partially integrated, meaning that their values on a finer mesh $\mathcal{M}_{n+k}$ are determined, up to expressions unresolved on this finer mesh. The RNG step 1, as implemented in this paper, is to express these terms, unresolved on $\mathcal{M}_n$, on successively finer grids $\mathcal{M}_{n+k}$.

In our treatment of step 2, we depart from conventional RNG methodology. We omit the remap step 2. For any finite number of steps, the remap is an isomorphism, and so its presence or absence is moot. However in the limit $k \to \infty$, there is a difference. The conventionally remapped RNG analysis would place the LES data at infinitely remote (spatial infinity) wave numbers to achieve the integration of a truly scale invariant problem. In the LES framework, we do not wish to eliminate the problem data in this manner, and so we forgo the remap and the RNG fixed point, while obtaining a RNG based series expansion for the unclosed $\mathcal{M}_n$ SGS terms. To emphasize this distinction, we refer to the limit we obtain as an RNG limit point (but not an RNG fixed point).

According to step 3, at each RNG step the equation parameters (the RNG relevant variables) should be set equal to the physical parameter values for that length scale. This must occur at the grid level $\mathcal{M}_{n+k}$.

We define turbulent and total dimensional transport parameters, the latter denoted $t_{\text{total}}$. We take the step 3 requirement to mean that the $N+1$ total (laminar plus turbulent) transport coefficients $t_{\text{total}} \in \mathcal{T}$ should be set at each RNG step. We could as well set the dimensionless transport coefficients. For this purpose, we follow convention and define $T_{\text{total}} = \nu_{\text{total}}/t_{\text{total}}$ as the dimensionless transport parameters. Sequences with different limit points $T_{\text{total}}(\text{Re} = \infty)$ for the dimensionless total transport should generate different infinite Re solutions of the Navier-Stokes or Euler equations.

Quantum field theory is the origin of the RNG method. Aside from intellectual and historical interest, examining commonalities of the use of similar ideas in widely varied contexts offers the chance to enrich both subject areas through exchange of information and techniques. In quantum field theory, the relevant variables (particle masses and coupling constants) are predicted neither by the RNG fixed point nor by the quantum field theory itself. The mass of the proton, a fundamental particle in strong coupling quantum field theory, is derived from an extended theory of quarks, in which the proton is not a fundamental particle but rather a derived object. More directly comparable is quantum electrodynamics. In principle, an exact integration of the RNG equation would give the observed (finite length scale) mass of the electron as a multiple of the bare (zero length scale) mass, but the bare mass is not known. We also compare to quantum chromodynamics (QCD). The similarity of QCD to turbulence RNG was previously noted [5]. QCD shares with turbulence theory an infrared fixed point, and the property that the coupling constant (the turbulent viscosity, for turbulence theory) becomes smaller at short length scales. This property of QCD is called asymptotic freedom. In turbulence theory, a similar exact integration of the RNG defines the turbulent diffusion coefficient as observed at finite length scales in terms of the same coefficient as observed at zero length scales. However, in contrast to quantum electrodynamics, this "bare" diffusion coefficient is generally accepted to be zero, thus is known. Moreover, for turbulent diffusion, the RNG integration is dominated by its low order perturbation term, and thus is effectively determined perturbatively, as with dynamic SGS models. Thus the dynamic LES turbulence theory of the infinite Re limit goes beyond the quantum field theory RNG in predicting its own coefficients.

### 2.3. Models and RNG relevant parameters

To set parameters according to RNG step 3 at the length scale of $\mathcal{M}_{n+k}$, we need observables at this same length scale, and with $N+1$ parameters to

be set, we need to specify $N+1$ observables, each an observable relative to the mesh $\mathcal{M}_{n+k}$. In other words, the observables should be functions of the averaged primitive variables on the mesh $\mathcal{M}_n$. These observables constitute the *model* for the unobserved SGS terms, and RNG step 3 supplies the (missing) coefficients for the model; i.e., it sets the coefficients for turbulent transport at each RNG step. In conventional RNG applications, the model coefficients are set by comparison to experimental data. Here they are set by theory. This coefficient specification is equivalent to specifying a point $T_{\text{total}} \in \mathcal{T}$ at each RNG step.

The coefficients for the SGS terms have the form $\nu_{\text{total}}/\text{Sc}_{\text{total}}$, $\nu_{\text{total}}/\text{Pr}_{total}$ and a similar ratio for the isotropic viscosity coefficient.

Dynamic LES is a single expansion step, $k=1$, of the RNG expansion. For this step, it contains the same steps 1 and 3 as the RNG and two additional steps:

4. Conventionally, we replace the continuous time but space discretized quantities of the RNG steps 1–3 with a time discretization as well. Thus the SGS terms are defined as the average over a time step of the cell face averages introduced below. To define a closed LES algorithm, we replace these unclosed SGS terms with the corresponding models multiplied by their coefficients as defined by step 3 in the numerical solution of the equations on the grid $\mathcal{M}_n$.
5. Model coefficients are determined by a theoretical analysis from the mesh level solutions to the governing equations.

In the RNG formalism, we label expansion terms at each order as irrelevant, relevant, or nonrenormalizable according to whether they become smaller, remain constant or grow as the renormalization map is iterated, and we consider the effects of finer grids as refinements of the grid $\mathcal{M}_n$. There should be no nonrenormalizable parameters. We anticipate $N+1$ relevant ones, namely the $N+1$ coefficients of the models, interpreted as dimensionless total transport coefficients.

Settings of the relevant parameters follow from the dynamic SGS analysis [29], a version of which is repeated here. This method specifies an Re-dependent path $T_{\text{turbulent}}(\text{Re}) \in \mathcal{T}$. These coefficients are combined with the laminar ones $T(\text{Re}) \in \mathcal{T}$ through a formula $t_{\text{total}} = t_{\text{turbulent}} + t_{\text{laminar}}$ and together define $T_{\text{total}}(\text{Re}) \in \mathcal{T}$ which uniquely specifies the LES method. The dynamic SGS method assumes a functional form for the model, and given that, derives the coefficients. Variations in this formalism can be based on alternate formulations for the model. The dynamic SGS method determines the coefficients of the model directly from the solutions at grid level $\mathcal{M}_n$ of the governing equations.

### 2.4. The scope and limitations of SGS/LES methods

The dynamic theory of SGS terms outlined above applies only to quadratic nonlinearities in the governing equations, giving rise to turbulent transport coefficients for viscosity, thermal conductivity and species concentration diffusion. Many important nonlinearities remain, and give rise to systematic difficulties in LES. Thermodynamic functions, such as pressure and temperature are obvious examples. Fluid transport (molecular level viscosity, thermal diffusion and species concentration diffusion) are also thermodynamic functions, and for plasmas, have strong nonlinearities. Radiation and material strength are additional potentially strong nonlinearities. This class of problems is known as subcell or mixed cell effective parameters. Such problems are often a serious complication to practical computations, and are not addressed through the LES/SGS methodology. As we will explain in Sec. 7, these problems are mitigated but not solved through use of Front Tracking.

## 3. Averaging procedure

The Reynolds-averaged equations associated with a system of conservation laws are obtained through application of a Reynolds averaging operator, such as ensemble averaging. Similarly, the equations that are discretized in an LES method arise from application of an integral operator, viz., convolution with a filter. Both a Reynolds averaging operator and convolution with a filter commute with spatial and temporal derivatives.

We prefer instead to use the averaging operator defined by volume integration over the cells of a spatial grid. Although the time derivative commutes such volume averaging, spatial derivatives do not. We compensate by viewing the cell averages of the solution of the conservation laws as solving a finite volume approximation to the system.

### 3.1. Discretized equations

Let us write the system of conservation laws under consideration as

$$\frac{\partial U}{\partial t} + \frac{\partial F_i(U)}{\partial x_i} = 0 \ , \tag{1}$$

where repeated tensor indices are summed. Here $U$ denotes the vector of densities of conserved quantities (e.g., mass, momentum, energy, and species). To this system we apply the cell averaging operator associated with a polygonal finite-volume mesh $\mathcal{M}$. For a cell $\mathcal{C}$ of $\mathcal{M}$, let $\overline{a}^{\mathcal{C}}$ denote the volume

integral over $\mathcal{C}$ of the quantity $a$ divided by the volume $V(\mathcal{C})$ of $\mathcal{C}$. By the divergence theorem, the volume integral over $\mathcal{C}$ of the divergence of the flux $F_i(U)$ equals the surface integral of the outward normal component of the flux over the boundary $\partial\mathcal{C}$. This boundary consists of the faces of the cell. If $f \subset \partial\mathcal{C}$ is a face of $\mathcal{C}$, let $\overline{b}^f$ denote the surface integral over $f$ of the quantity $b$ divided by the surface area $A(f)$ of $f$. Then averaging Eq. (1) over the cell $\mathcal{C}$ yields the semi-discrete evolution equation

$$\frac{\mathrm{d}\overline{U}^{\mathcal{C}}}{\mathrm{d}t} + \sum_{\{f \subset \partial\mathcal{C}: f \text{ a face of } \mathcal{M}_\setminus\}} \frac{A(f)}{V(\mathcal{C})}\, n_i^{\mathcal{C},f}\, \overline{F_i(U)}^f = 0 \ , \tag{2}$$

where $n_i^{\mathcal{C},f}$ is the unit normal to face $f$ pointing outward from $\mathcal{C}$.

The face-averaged flux $\overline{F_i(U)}^f$ is constructed as follows. First, we write

$$\overline{F_i(U)}^f = F_i(\overline{U}^f) + F_i^{f,\mathrm{SGS}}(U) \ . \tag{3}$$

This equation defines the SGS flux $F_i^{f,\mathrm{SGS}}(U)$. Explicit formulae for the SGS flux components for compressible mixing are given in Sec. 4; an expansion for each SGS term, which is the central result of the present paper, is developed in Sec. 5. Second, $F_i(\overline{U}^f)$ is related to cell-averaged conserved quantities through a numerical scheme, such as

$$n_i^{\mathcal{C},f} F_i(\overline{U}^f) = \mathcal{F}(\overline{U}^{\mathcal{C}}, \overline{U}^{\mathcal{C}'}, n^{\mathcal{C},f}) + \mathcal{E}^{\mathcal{C},f}(U) \ , \tag{4}$$

$\mathcal{C}'$ being the cell sharing face $f$ with $\mathcal{C}$. Here $\mathcal{F}$ is the numerical flux for a conservative, consistent finite-volume scheme and $\mathcal{E}^{\mathcal{C},f}$ is its truncation error, discussed in Sec. 7.

### 3.2. Projection operators

To be more concrete, we focus on cubic meshes. That is, we take the physical domain to be $\mathcal{D} = [0,1]^D$, the $D$-dimensional unit cube with periodic boundary conditions, and we let $\mathcal{M}_n$ be the cubic mesh with a corner at the origin that divides $\mathcal{D}$ into equal sized cells, each with edge lengths $2^{-n}$. Thus $\mathcal{M}_{n+1}$, $\mathcal{M}_{n+2}$, ... are nested refinements of the base mesh $\mathcal{M}_n$, which remains fixed throughout the discussion.

Let $E_n$ be the operation of averaging over faces of the grid $\mathcal{M}_n$. Applied to a function $a$ defined on $\mathcal{F}_n$ (the union of the faces of $\mathcal{M}_n$), this operation yields a piecewise-constant function $E_n\, a$ that is constant over each face, the

constant value for face $f$ being its average $\overline{a}^f$ over the face. On the Hilbert space $\mathcal{H}_n = L^2(\mathcal{F}_n, \mathrm{d}^{D-1}x)$, the operator $E_n$ is an orthogonal projection onto the subspace $E_n\mathcal{H}_n$ comprising such piecewise-constant functions. In fact for face $f$,

$$\overline{a}^f = \frac{\int_f a\,\mathrm{d}^{D-1}x}{\int_f \mathrm{d}^{D-1}x} = \frac{\langle 1_f, a\rangle}{\langle 1_f, 1_f\rangle}\ , \tag{5}$$

where $1_f$ is the characteristic function of $f$, which takes the value 1 on $f$ and zero elsewhere, and the brackets $\langle\cdot,\cdot\rangle$ denote the usual inner product on $\mathcal{H}_n$. Therefore

$$E_n\, a == \sum_{\{f\subset\mathcal{F}_n : f \text{a face of } \mathcal{M}_\backslash\}} \overline{a}^f\, 1_f = \sum_{\{f\subset\mathcal{F}_n : f \text{a face of } \mathcal{M}_\backslash\}} \frac{1_f\,\langle 1_f, a\rangle}{\langle 1_f, 1_f\rangle}\ . \tag{6}$$

Let $F_n = I - E_n$ denote the complementary projection operator. When the choice of mesh is unambiguous, we write $\overline{a}$ in place of the mean $E_n\, a$ and $a' = a - \overline{a}$ in place of the fluctuation $F_n\, a$.

In addition to the simple averaging operator $E_n$, the mass density-weighted, or Favre, averaging operator $\widetilde{E}_n$ is useful. We assume that $\rho$ has sufficient regularity to allow its restriction to the faces of $\mathcal{M}_n$ and, as restricted, to being locally integrable. On the Hilbert space $\widetilde{\mathcal{H}}_n = L^2(\mathcal{F}_n, \rho\,\mathrm{d}^{D-1}x)$, the operator $\widetilde{E}_n$ is likewise an orthogonal projection onto the subspace $\widetilde{E}_n\widetilde{\mathcal{H}}_n$. For face $f$

$$\widetilde{a}^f = \frac{\overline{\rho a}^f}{\overline{\rho}^f} = \frac{\int_f a\rho\,\mathrm{d}^{D-1}x}{\int_f \rho\,\mathrm{d}^{D-1}x} = \frac{\langle 1_f, a\rangle_\rho}{\langle 1_f, 1_f\rangle_\rho}\ , \tag{7}$$

where the notation $\langle\cdot,\cdot\rangle_\rho$ stands for the usual inner product on $\widetilde{\mathcal{H}}_n$. Hence

$$\widetilde{E}_n\, a = \sum_{f\subset\mathcal{F}_n} \frac{1_f\,\langle 1_f, a\rangle_\rho}{\langle 1_f, 1_f\rangle_\rho}\ . \tag{8}$$

We also let $\widetilde{F}_n = I - \widetilde{E}_n$ and, when unambiguous, denote the Favre mean $\widetilde{E}_n\, a$ by $\widetilde{a}$ and the Favre fluctuation $\widetilde{F}_n\, a$ by $a'' = a - \widetilde{a}$.

For $k = 1, 2, \ldots$, the projection operator $\widetilde{E}_{n+k}$ on $\widetilde{\mathcal{H}}_{n+k} = L^2(\mathcal{F}_{n+k}, \rho\,\mathrm{d}^{D-1}x)$ is defined similarly. However, we shall regard $\widetilde{E}_{n+k}$ instead as the operator on $\widetilde{\mathcal{H}}_n$ that acts in the following way on $a \in \widetilde{\mathcal{H}}_n$: first extend $a$ to all of the faces of $\mathcal{M}_{n+k}$, setting it to zero except on the faces of $\mathcal{M}_n$; next apply $\widetilde{E}_{n+k}$; and finally restrict the result to the faces of $\mathcal{M}_n$, obtaining $\widetilde{E}_{n+k}\, a \in \widetilde{\mathcal{H}}_n$. The operator $\widetilde{E}_{n+k}$ so defined is a projection operator on $\widetilde{\mathcal{H}}_n$.

Thus $\widetilde{E}_{n+k}\widetilde{\mathcal{H}}_n$ consists of square-integrable functions defined on $\mathcal{F}_n$ that are constant on each face of $\mathcal{M}_{n+k}$ contained within a face of $\mathcal{M}_n$.

We note an operator identity that will be useful:

$$\widetilde{E}_n = \widetilde{E}_n \widetilde{E}_{n+1} \ . \tag{9}$$

Also, because $\widetilde{E}_n$ is a projection operator given by Eq. (8),

$$\langle 1_f, a\, \widetilde{E_n}\, b\rangle_\rho = \langle \widetilde{E_n}(1_f\, a), \widetilde{E_n}\, b\rangle_\rho = \langle 1_f, (\widetilde{E_n}\, a)\, \widetilde{E_n}\, b\rangle_\rho \ , \tag{10}$$

so that

$$\widetilde{E}_n \left[a\, \widetilde{E}_n\, b\right] = \widetilde{E}_n \left[(\widetilde{E}_n\, a)\, \widetilde{E}_n\, b\right] \ . \tag{11}$$

## 4. Averaged equations for compressible mixing

To illustrate the SGS flux defined by Eq. (3), we describe the flux in detail for the system of conservation laws governing the compressible mixing of two gases.

The state of an ideal mixture of two polytropic gases is characterized by the field variables $\rho$, $v_i$, $T$ and $\psi$, which denote the mass density, particle velocity vector, temperature and mass fraction, respectively. The mixture has pressure $p = \rho RT$, where $R = \psi R_1 + (1-\psi)R_2$, and specific internal energy $e = c_v T$, where $c_v = \psi\, c_{v,1} + (1-\psi)\, c_{v,2}$. Here $R_\alpha = N_A k_B / M_\alpha$ and $c_{v,\alpha}$ are constants for $\alpha = 1, 2$. The specific total energy is denoted $E = \frac{1}{2} v_\ell v_\ell + e$. The specific enthalpy of the mixture is $h = e + p/\rho = c_p T$ with $c_p = c_v + R$, and the individual specific enthalpies for the two gases are $h_\alpha = c_{p,\alpha} T$, where $c_{p,\alpha} = c_{v,\alpha} + R_\alpha$.

The laminar transport coefficients for momentum, heat, and mass are the kinematic anisotropic and isotropic viscosities, $\nu$ and $\nu_{\rm i}$, thermal diffusivity $\kappa = \nu/{\rm Pr}$ and mass diffusivity $D = \nu/{\rm Sc}$, where Pr and Sc denote the Prandtl and Schmidt parameters. The viscous stress tensor, heat flux vector, and diffusive mass flux vector are

$$\sigma^{\rm v}_{ij} = \rho\nu_{\rm i} \frac{\partial v_\ell}{\partial x_\ell}\, \delta_{ij} + \rho\nu \left( \frac{\partial v_i}{\partial x_j} + \frac{\partial v_j}{\partial x_i} - \frac{2}{3} \frac{\partial v_\ell}{\partial x_\ell}\, \delta_{ij} \right) \ , \tag{12}$$

$$q_i = -\rho\kappa c_p \frac{\partial T}{\partial x_i} \ , \tag{13}$$

$$j_i = -\rho D \frac{\partial \psi}{\partial x_i} \ . \tag{14}$$

For simplicity, $\rho\nu$, $\rho\nu_{\rm i}$, $\rho\kappa$ and $\rho D$ (hence $\nu/\nu_{\rm i}$, Pr and Sc) are assumed to be constant.

The cell-averaged laws of conservation of mass, momentum, energy and species, which govern the averaged field variables $\overline{\rho}$, $\widetilde{v_i}$, $\widetilde{T}$ and $\widetilde{\psi}$, are

$$\frac{\partial\,\overline{\rho}}{\partial t}+\frac{\partial\,\overline{\rho}\,\widetilde{v_i}}{\partial x_i}=0\ , \tag{15}$$

$$\frac{\partial\,\overline{\rho}\,\widetilde{v_j}}{\partial t}+\frac{\partial(\overline{\rho}\,\widetilde{v_i}\,\widetilde{v_j}+\overline{p}\,\delta_{ij})}{\partial x_i}=\frac{\partial\overline{\sigma^{\rm v}_{ij}}}{\partial x_i}-\frac{\partial\tau_{ij}}{\partial x_i}\ , \tag{16}$$

$$\begin{aligned}\frac{\partial\,\overline{\rho}\widetilde{E}}{\partial t}+\frac{\partial(\overline{\rho}\widetilde{E}+\overline{p})\,\widetilde{v_i}}{\partial x_i}&=\frac{\partial\overline{\sigma^{\rm v}_{ij}}\,\widetilde{v_j}}{\partial x_i}-\frac{\partial\overline{q_i}}{\partial x_i}-\frac{\partial(\widetilde{h_1}-\widetilde{h_2})\,\overline{j_i}}{\partial x_i}\\&\quad-\frac{\partial\tau_{ij}\widetilde{v_j}}{\partial x_i}-\frac{\partial q_i^{(h)}}{\partial x_i}-\frac{\partial q_i^{(h\psi)}}{\partial x_i}-\frac{\partial q_i^{(k)}}{\partial x_i}-\frac{\partial q_i^{(\rm v)}}{\partial x_i}\ ,\end{aligned} \tag{17}$$

$$\frac{\partial\,\overline{\rho}\,\widetilde{\psi}}{\partial t}+\frac{\partial\,\overline{\rho}\,\widetilde{\psi}\,\widetilde{v_i}}{\partial x_i}=-\frac{\partial\overline{j_i}}{\partial x_i}-\frac{\partial q_i^{(\psi)}}{\partial x_i}\ . \tag{18}$$

For clarity, we have made the formal replacement (which is actually an identity in the sense of distribution derivatives)

$$\sum_{\{f\subset\partial\mathcal{C}:f\text{is a face of}\mathcal{M}_\setminus\}}\frac{A(f)}{V(\mathcal{C})}\,n_i^{\mathcal{C},f}\mapsto\frac{\partial}{\partial x_i} \tag{19}$$

in Eq. (2) and omitted the $\mathcal{C}$ and $f$ indications on the averaging operators. (An average of a field variable appearing within a time derivative is a cell average, whereas within a spatial derivative it is a face average.)

Appearing in Eqs. (15)–(18) are the SGS flux components $\tau_{ij}$, $q_i^{(h)}$, $q_i^{(h\psi)}$, $q_i^{(k)}$, $q_i^{(\rm v)}$ and $q_i^{(\psi)}$, which are defined by

$$\tau_{ij}=\overline{\rho}\,(\widetilde{v_i\,v_j}-\widetilde{v_i}\,\widetilde{v_j})=\overline{\rho}\,\widetilde{v_i''\,v_j''}\ , \tag{20}$$

$$\begin{aligned}q_i^{(h)}&=\overline{\rho}\left(\widetilde{h\,v_i}-\widetilde{h}\,\widetilde{v_i}\right)\\&=\overline{\rho}\,\widetilde{c_p}\,\widetilde{T''\,v_i''}+\overline{\rho}\,(c_{p,1}-c_{p,2})\left(\widetilde{T}\,\widetilde{\psi''\,v_i''}+\widetilde{\psi''\,T''}\,\widetilde{v_i''}\right)\ ,\end{aligned} \tag{21}$$

$$q_i^{(h\psi)}=\overline{(h_1-h_2)\,j_i}-(\widetilde{h_1}-\widetilde{h_2})\,\overline{j_i}=(c_{p,1}-c_{p,2})\left(\overline{T''}\ \overline{j_i}+\overline{T'j_i'}\right)\ , \tag{22}$$

$$q_i^{(k)}=\tfrac{1}{2}\overline{\rho}\left(\widetilde{v_\ell\,v_\ell\,v_i}-2\,\widetilde{v_\ell}\,\widetilde{v_\ell\,v_i}-\widetilde{v_\ell\,v_\ell}\,\widetilde{v_i}+2\,\widetilde{v_\ell}\,\widetilde{v_\ell}\,\widetilde{v_i}\right)=\tfrac{1}{2}\overline{\rho}\,\widetilde{v_\ell''\,v_\ell''\,v_i''}\ , \tag{23}$$

$$q_i^{(\rm v)}=-\left(\overline{\sigma^{\rm v}_{ij}\,v_j}-\overline{\sigma^{\rm v}_{ij}}\,\widetilde{v_j}\right)=-\overline{\sigma^{\rm v}_{ij}}\ \overline{v_j''}-\overline{(\sigma^{\rm v}_{ij})'\,v_j'}\ , \tag{24}$$

$$q_i^{(\psi)}=\overline{\rho}\left(\widetilde{\psi\,v_i}-\widetilde{\psi}\,\widetilde{v_i}\right)=\overline{\rho}\,\widetilde{\psi''\,v_i''}\ . \tag{25}$$

Here we have taken advantage of the properties $\overline{a'} = 0$ and $\widetilde{a''} = 0$ of cell and face averaging (but not convolution with a filter).

A related SGS quantity, the fluctuation kinetic energy $k$ defined by $\overline{\rho}\, k = \frac{1}{2}\tau_{\ell\ell} = \frac{1}{2}\overline{\rho}\,\widetilde{v''_\ell\, v''_\ell}$, arises in the formula $\widetilde{E} = \frac{1}{2}\widetilde{v}_\ell\,\widetilde{v}_\ell + \widetilde{e} + k$. The Favre-averaged specific internal energy $\widetilde{e}$ is viewed as $\widetilde{c_v}\widetilde{T}$ plus the SGS term $\widetilde{c_v T} - \widetilde{c_v}\widetilde{T} = (c_{v,1} - c_{v,2})\,\widetilde{\psi'' T''}$; and the averaged pressure $\overline{p} = \overline{\rho}\widetilde{R T}$ occurring in the conservation laws is treated similarly. Also, in $\overline{j_i} = -\rho D\,\partial\overline{\psi}/\partial x_i$, the variable $\overline{\psi}$ should be replaced by $\widetilde{\psi}$ plus the SGS term $\overline{\psi''}$; similarly, the SGS terms $\overline{v''_\ell}$ and $\overline{T''}$ enter into $\overline{\sigma^{\mathrm{v}}_{ij}}$ and $\overline{q_i}$, respectively. Notice that a quantity such as $\overline{\psi''}$ is equivalently written as $\overline{\rho}\,\widetilde{(\rho^{-1})''\,\psi''}$.

Thus we see that an SGS term for the compressible mixing of two gases, under the stated modeling assumptions, involves either a covariance $\mathrm{cov}(a,b) = \overline{a'\,b'}$, a Favre covariance $\widetilde{\mathrm{cov}}(a,b) = \widetilde{a''\,b''}$, or a third-order Favre cumulant $\widetilde{\mathrm{cum}}(a,b,c) = \widetilde{a''\,b''\,c''}$, where $a$, $b$ and $c$ are each one of $\rho^{-1}$, $v_i$, $T$ or $\psi$ or their spatial derivatives.

## 5. Expansions for SGS terms

The flux appearing in the discretized conservation laws (2) is decomposed, via Eq. (3), into a function of $\overline{U} = E_n U$ plus the SGS flux. A function of $E_n U$ is said to be resolved on $\mathcal{M}_n$. In this section we develop expansions for SGS terms involving quantities that are resolved on successively finer grids.

### 5.1. Leonard SGS term

A familiar SGS term is the Reynolds stress tensor $\tau^{(n)}_{ij}$, where

$$\tau^{(n)}_{ij} = \overline{\rho\, v_i\, v_j} - \overline{\rho\, v_i}\;\overline{\rho\, v_j}/\overline{\rho}\;. \tag{26}$$

The superscript $n$ indicates that the averaging occurs on the grid $\mathcal{M}_n$. Consider the corresponding tensor $\tau^{(n-1)}_{ij} = \widehat{\rho\, v_i\, v_j} - \widehat{\rho\, v_i}\;\widehat{\rho\, v_j}/\widehat{\rho}$ on the once-coarsened grid $\mathcal{M}_{n-1}$, where the caret denotes averaging for $\mathcal{M}_{n-1}$, and compare it with $\tau^{(n)}_{ij}$, as averaged onto $\mathcal{M}_{n-1}$. The Germano identity [8] is that the difference $\tau^{(n-1)}_{ij} - \widehat{\tau^{(n)}_{ij}}$ between these two $\mathcal{M}_n$-unresolved SGS terms reduces to the Leonard stress tensor [19, 29, 24]

$$\mathcal{L}^{(n-1)}_{ij} = \widehat{\overline{\rho}\,\widetilde{v}_i\,\widetilde{v}_j} - \widehat{\overline{\rho}\,\widetilde{v}_i}\;\widehat{\overline{\rho}\,\widetilde{v}_j}/\widehat{\overline{\rho}}\;, \tag{27}$$

which is resolved on $\mathcal{M}_n$. The reduction occurs because of the cancellation of the two terms, $\widehat{\rho\, v_i\, v_j}$ and $\widehat{\overline{\rho\, v_i\, v_j}}$, that are not $\mathcal{M}_n$-resolved.

### 5.2. Generalized Leonard SGS term

More generally, consider an SGS term in the form of a Favre covariance

$$\widetilde{\mathrm{cov}}_n(a,b) = \widetilde{a''\,b''} = \widetilde{a\,b''} = \widetilde{E}_n\left[a\,\widetilde{F}_n\,b\right] \tag{28}$$

of the quantities $a$ and $b$ with respect to the mesh $\mathcal{M}_n$. (The ordinary covariance $\mathrm{cov}_n(a,b) = \overline{a'\,b'}$ is included as a special case.) By analogy, we define the corresponding Leonard SGS term to be

$$\widetilde{\mathcal{L}}_n(a,b) = \widetilde{\mathrm{cov}}_n(a,b) - \widetilde{E}_n\,\widetilde{\mathrm{cov}}_{n+1}(a,b)\ . \tag{29}$$

As we now demonstrate, this quantity is $\mathcal{M}_{n+1}$-resolved provided that $\rho\,a$ and $\rho\,b$ are components of $U$.

Using the identity (28) on levels $n$ and $n+1$, along with the operator identity (9) and the definitions $\widetilde{F}_n = I - \widetilde{E}_n$ and $\widetilde{F}_{n+1} = I - \widetilde{E}_{n+1}$, we see that

$$\begin{aligned}\widetilde{\mathcal{L}}_n(a,b) &= \widetilde{E}_n\left[a\,\widetilde{F}_n\,b\right] - \widetilde{E}_n\widetilde{E}_{n+1}\left[a\,\widetilde{F}_{n+1}\,b\right]\\ &= \widetilde{E}_n\left[a\,(\widetilde{E}_{n+1} - \widetilde{E}_n)\,b\right]\ .\end{aligned} \tag{30}$$

By identity (9) again along with Eq. (11) at levels $n$ and $n+1$,

$$\widetilde{\mathcal{L}}_n(a,b) = \widetilde{E}_n\left[(\widetilde{E}_{n+1}\,a)\,\widetilde{E}_{n+1}\,b\right] - \widetilde{E}_n\left[(\widetilde{E}_n\,a)\,\widetilde{E}_n\,b\right]\ . \tag{31}$$

Finally, according to identity (9), an $\mathcal{M}_n$-resolved quantity is also $\mathcal{M}_{n+1}$-resolved. Hence $\widetilde{\mathcal{L}}_n(a,b)$ is $\mathcal{M}_{n+1}$-resolved.

### 5.3. Expansion for a covariance

Next we develop an expansion for the Favre covariance $\widetilde{\mathrm{cov}}_n(a,b) = \widetilde{a''\,b''}$. By definition of the generalized Leonard SGS term,

$$\widetilde{\mathrm{cov}}_n(a,b) = \widetilde{\mathcal{L}}_n(a,b) + \widetilde{E}_n\,\widetilde{\mathrm{cov}}_{n+1}(a,b)\ . \tag{32}$$

By induction on $n$, we see that

$$\widetilde{\mathrm{cov}}_n(a,b) = \widetilde{E}_n\sum_{j=0}^{J}\widetilde{\mathcal{L}}_{n+j}(a,b) + \widetilde{E}_n\,\widetilde{\mathrm{cov}}_{n+J+1}(a,b)\ . \tag{33}$$

The sum involving Leonard terms, which we denote by $\widetilde{\mathrm{cov}}_{n,J}(a,b)$, is resolved on the grid $\mathcal{M}_{n+J+1}$. The remainder is denoted by $R_{n,J}(a,b)$.

### 5.4. Expansion for a third-order cumulant

Some of the SGS terms in system (15)–(18) involve third-order cumulants, such as $\widetilde{\psi'' T'' v_i''}$ and $\widetilde{v_\ell'' v_\ell'' v_i''}$. The presence of fluctuations indicates that these terms are not $\mathcal{M}_n$-resolved; and because they are not covariances, they are not handled by the methods of Sec. 5.3. Our procedure is to expand each fluctuation factor as an average plus a fluctuation relative to $\mathcal{M}_{n+1}$, and after organizing and simplifying the result, we iterate and generate the expansion with remainder to all orders.

The expansion step is to replace each of the $\widetilde{F}_n$ operators in the general third-order cumulant,

$$\widetilde{\mathrm{cum}}_n(a,b,c) = \widetilde{a'' b'' c''} = \widetilde{E}_n \left[ (\widetilde{F}_n a)\,(\widetilde{F}_n b)\,(\widetilde{F}_n c) \right] , \tag{34}$$

using the identity

$$\widetilde{F}_n = \left( \widetilde{E}_{n+1} - \widetilde{E}_n \right) + \widetilde{F}_{n+1} . \tag{35}$$

Let the quantity in parentheses be denoted by $\widetilde{F}_{n,1}$. The expansion generates eight terms. The term

$$\widetilde{\mathrm{cum}}_{n,1}(a,b,c) = \widetilde{E}_n \left[ (\widetilde{F}_{n,1}\, a)\,(\widetilde{F}_{n,1}\, b)\,(\widetilde{F}_{n,1}\, c) \right] \tag{36}$$

from which $\widetilde{F}_{n+1}$ is absent is the leading order of the expansion. The seven terms with one, two or three $\widetilde{F}_{n+1}$ operators constitute the remainder term, $\widetilde{R}_{n,1}(a,b,c)$. In fact, the terms in $\widetilde{R}_{n,1}(a,b,c)$ with one $\widetilde{F}_{n+1}$ are zero as they each involve a fluctuation averaged against the product of two constant states; thus there are four non-zero remainder terms.

To continue this expansion of $\widetilde{a'' b'' c''}$, we employ the operator identity

$$\widetilde{F}_n = \left( \widetilde{E}_{n+J+1} - \widetilde{E}_n \right) + \widetilde{F}_{n+J+1} . \tag{37}$$

With the quantity in parentheses in the preceding equation denoted by $\widetilde{F}_{n,J}$,

$$\widetilde{\mathrm{cum}}_n(a,b,c) = \widetilde{E}_n \left[ (\widetilde{F}_{n,J}\, a)\,(\widetilde{F}_{n,J}\, b)\,(\widetilde{F}_{n,J}\, c) \right] + \widetilde{R}_{n,J}(a,b,c) , \tag{38}$$

where the remainder $\widetilde{R}_{n,J}(a,b,c)$ comprises the four nonzero terms involving the operator $\widetilde{F}_{n+J+1}$. The first term in Eq. (38), which we denote by $\widetilde{\mathrm{cum}}_{n,J}(a,b,c)$, is resolved on the grid $\mathcal{M}_{n+J+1}$.

## 6. Numerical modeling

The discretized system of conservation laws, Eqs. (2)–(4), involve the SGS flux, defined by Eq. (3), which depends in an essential way on the solution $U$, not solely on the face average $\overline{U} = E_n U$. To close the governing system of equations, each SGS term must be related to the face average of the solution through a closure relation. In dynamic SGS modeling, the closure relation is determined with the aid of the Leonard SGS term.

### 6.1. Dynamic SGS modeling

We assume that the replacement for the SGS term for the grid level $\mathcal{M}_n$ takes the form $c_n M_n$ for some coefficient sequence $c_n$. Here $M_n$, is called the model for the particular SGS term. It is required to be a function of the cell averages of the primitive quantities in the dynamic equations, so that the expression for $M_n$ "closes". Furthermore, we make the asymptotic assumption that $c_n$ converges as $n \to \infty$, so that $c_n$ is approximately independent of $n$ when $n$ is large. The limit, denoted $c$, is the turbulent transport coefficient. For instance, when the SGS term is $\widetilde{\mathrm{cov}}_n(a,b)$, the closure, or modeling, relation is

$$\widetilde{\mathrm{cov}}_n(a,b) \approx c\, M_n \ . \tag{39}$$

If $\widetilde{\mathrm{cov}}_n(a,b)$ is a tensor quantity, so is the corresponding model $M_n$, and distinct coefficients are used for the deviatoric and spherical parts of this relationship.

Determination of the turbulent transport coefficient $c$ (LES step 5 in Sec. 2.3) proceeds as follows. Because the same coefficient $c$ relates the SGS term to the model at both grid levels $\mathcal{M}_{n-1}$ and $\mathcal{M}_n$, the difference $M_{n-1} - \widetilde{E}_{n-1} M_n$ is a model for the Leonard SGS term $\widetilde{\mathcal{L}}_{n-1}(a,b)$. We therefore compute $c$ by requiring that

$$\widetilde{\mathcal{L}}_{n-1}(a,b) \approx c \left( M_{n-1} - \widetilde{E}_{n-1} M_n \right) \ . \tag{40}$$

All expressions in Eq. (40), other than $c$, are $\mathcal{M}_n$-resolved. Thus, using (40), $c$ is also. For tensor SGS terms, $c$ is a scalar and (40) is interpreted in the sense of least squares.

The cancellation of terms in $\widetilde{\mathcal{L}}_{n-1}(a,b)$ is exact, whereas the assumption that $\widetilde{\mathrm{cov}}_n(a,b)$ is proportional to the model $M_n$ is an ansatz or approximation. The choice of model remains open for experimentation and improvement. Once the model has been specified, Eq. (40) determines the coefficient $c$ dynamically from the solution.

In keeping with the discussion in Sec. 2.3 regarding choice of renormalization length scales, the turbulent transport coefficients of all SGS terms, excepting the anisotropic viscous term, are taken to be proportional to the anisotropic turbulent viscosity, with a dimensionless coefficient of proportionality.

### 6.2. Third-order cumulants and higher order expansion terms

We believe the closed form expansion terms derived here for the unclosed SGS terms is new and could aid in future efforts to improve modeling of closure terms. In the cubic expansion, there are four remainder terms, three with two $\widetilde{F}_{n+1}$ and one with three of them. The Leonard stress is again a difference, arranged so that unobserved terms cancel and models proportional to Leonard stress terms are solvable in a current grid level. We are not aware of any effort to build a model for cubic or higher order quadratic expansion terms out of grid averaged primitive variables. If one imagines a higher order LES closure, in which the quadratic terms have their own dynamic equations, and thus become primitive variables, then the construction of models for cubic expansion terms can be constructed from the quadratic averaged variables. Similarly, higher order expansion terms appear to be naturally related to higher order LES closures. We do not go into details. We form a similar difference of SGS stress terms, out of the cubic terms, as was done for the quadratic case. Thus we form the difference of the $J$th expansion starting at $n-J-1$ with the $\widetilde{E}_{n-1}$ projection of the $J$th expansion, starting at $n-J$. For the first, we substitute $n-J-1$ for $N$ in (38). For the second, which is subtracted from the first, we substitute $n-J$ for $n$ in (38). We need to show that the difference is $\mathcal{M}_n$-resolved. For this purpose it is sufficient to look at the differences of the remainders of these expansions. Each remainder has $J$ expansion steps and $J$ mesh levels of $\widetilde{F}$ factors. The specific mesh levels and factors are shifted by one unit in the two terms of the difference, and it is these distinct mesh level factors at the beginning and end of the finite expansions that we examine. For each, we "undo" the basic expansion step, replacing $\widetilde{F}$s with a sum of $I$ and the corresponding $\widetilde{E}$. The difference with the $I$ inserted cancels, and the difference (or the individual terms) with the $\widetilde{E}$ inserted is $\mathcal{M}_n$-resolved. Thus we see that the cubic higher order Leonard

term is $\mathcal{M}_n$-resolved. Subject to the construction of a suitable higher order model, the higher order model coefficient can be determined.

### 6.3. The leading order RNG expansion

To leading order, we consider a single RNG step. With the current grid level denoted $\mathcal{M} = \mathcal{M}_n$, we also consider the once refined grid $\mathcal{M}_{n+1}$, for which each cell has been refined once in each mesh direction. On the cell faces of $\mathcal{M}_n$, we consider functions which are piecewise constant on cell faces of $\mathcal{M}_{n+1}$. In all cases, the leading order contribution to the unclosed SGS term is a product of two or more differences of primitive variables multiplied by an expression depending on $\rho$ and perhaps other variables which are not differenced. The differences occur in one or both of the directions tangential to the face of the grid cell. Detailed evaluation of these terms offers possible improvement for SGS modeling.

## 7. The LES/SGS/FT algorithm: V&V

Without question, turbulence and turbulent mixing are important problems for scientific computing and play a central role in modern engineering design. Validation of these simulations (comparison to experiment) is an essential part of the scientific method. With nonunique and algorithmically dependent numerical solutions, validation is hardly possible and instead, robust engineering design relies on calibration, which depends intrinsically on a sufficient range of experiments in a neighborhood of a design point.

We see a tight linkage between SGS terms and a cure for possible numerical nonuniqueness. Solutions are observed to vary as a consequence of variation of the SGS terms. Omission of these terms or the inclusion of transport related algorithmic artifacts leads to a variation in the solution, i.e., nonuniqueness. Thus we find that specification of the SGS terms in combination with control over diffusion related numerical artifacts removes the nonuniqueness. Nonuniqueness has its ultimate origin in the numerical miss-specification of fluid transport. In the present case, with molecular transport added according to the laws of physics, it is the turbulent and numerical transport which gives rise to nonuniqueness of solutions. The SGS terms, which specify subgrid turbulent transport, and front tracking to reduce numerical diffusion restore uniqueness. It remains to show that this choice (dynamic SGS terms and control over numerical mass diffusion) satisfies the standards of V&V.

Nonuniqueness is a strictly mathematical verification issue. Within the study of turbulence, the sensitivity of solutions to turbulence models is ubiquitous. Numerical nonuniqueness for the high Re limit has been demon-

strated by the wide range of simulation results obtained for a single high Re turbulent mixing problem [4]. Code comparison [25] of apparently converged solutions showed differences in thermal mixing properties. Additionally, systematic variation of the SGS coefficient has been observed to change the atomic mixing properties of nominally converged solutions [27]. Consistent with these observations are the comments [10]: "Results using the MILES approach for LES are found to strongly depend on scheme parameters and grid size. Also, physical variables cannot be simultaneously predicted." See also [33, 6, 1].

### 7.1. Verification and validation

In Table 1, we summarize the observed numerical and experimental variation in efforts to determine the overall growth rate $\alpha$ of the Rayleigh-Taylor instability mixing zone (MZ) width. Note the good validation results which have been achieved using FT/LES/SGS, particle methods and DNS (see Table 2). The Rayleigh-Taylor (RT) experiments give unique $\alpha$ values, i.e., they are appear to be repeatable (we allocate the 5–30% experimental variation in RT $\alpha$ predominantly to variation in recorded experimental conditions, in keeping with our simulations which duplicate the experiment to experiment variation in $\alpha$), so that any solution (such as the FT/LES/SGS solution) which agrees with these experiments is itself numerically unique.

In [27], we outline a validation/verification program for LES in the high Re regime, based on the code FT/LES/SGS. The LES/SGS framework has no adjustable parameters. Our validation is in the RT experimental regime. We have validated the FT/LES/SGS code by comparison to experimental measurements of the RT growth rate $\alpha$, conducted at $\mathrm{Re} \sim 3.5 \times 10^4$. Extrapolation to larger or infinite values of Re is treated as a perturbation with the small expansion parameter 1/Re and analyzed by simulation methods (verification). This validation tests the transport coefficients, which in the LES/SGS framework, are not adjustable, and which are much more sensitive in the RT experiments than in the Richtmyer-Meshkov (RM) experiments. Additionally, FT has been compared to RAGE [25] for RM problems and so we rely on the RM validation of RAGE.

We have conducted extensive studies of RT instabilities, as V&V for the FT/LES/SGS algorithm. Expanding on the bottom two lines of Table 1, we summarize the principal results in Table 2. For completeness, DNS and particle method simulations, which also show agreement with experiment, are included. We observe nearly perfect agreement between simulation and experiment, within error bars, and accuracy sufficient to distinguish between the distinct alphas of distinct experiments. In this way, we show that the

Table 1: Variabilities in $\alpha$ from a variety of experimental and numerical sources

| Experimental variabilities | |
|---|---|
| Due to initial conditions | 5–30% |
| Due to experimental fluid transport properties | 20% |
| Numerical issues: ILES | |
| ILES to experiment discrepancy [4] | 100% |
| ILES to ILES simulation discrepancy [4] | 50% |
| Numerical issues: LES/SGS/FT | |
| Numerical variation from transport coefficients [20, 21] | 5% |
| FT/LES/SGS to experiment discrepancy [21] | 5% |

Table 2: Comparison of FT simulation to experiment, for the RT growth rate $\alpha$. Discrepancy refers to the comparison of results outside of uncertainty intervals, if any, as reported

| Ref. | Exp. | Sim. Ref. | $\alpha_{\text{exp}}$ | $\alpha_{\text{sim}}$ | Discrepancy |
|---|---|---|---|---|---|
| LES/SGS/FT | | | | | |
| [38] | #112 | [20] | 0.052 | 0.055 | 6% |
| [38] | #105 | [9] | 0.072 | $0.076 \pm 0.004$ | 0% |
| [38, 36] | 10 exp. | [7] | 0.055–0.077 | 0.066 | 0% |
| [34] | air-He | [23] | 0.065–0.07 | 0.069 | 0% |
| [31] | hot-cold | [20, 9] | $0.070 \pm 0.011$ | 0.075 | 0% |
| [32] | salt-fresh | [9] | $0.085 \pm 0.005$ | 0.084 | 0% |
| DNS | | | | | |
| [31] | hot-cold | [31] | $0.070 \pm 0.011$ | $\sim 0.070$ | 0% |
| Particle Methods | | | | | |
| [12] | | [12] | | $0.06 \pm 0.005$ | |

variation in $\alpha$ across multiple experiments is caused partly by initial conditions (the water channel splitter plate experiments introduce significant noise) and partly by changes in the fluid transport properties of the fluids [20, 21]. The common belief that significant long wave length noise present in the initial data explains the factor of two discrepancy between experiment and the numerous ILES simulations, has been shown to be false [9]. The effect on $\alpha$ from the long wave length perturbations in the initial condition of [38] was shown [9] to be $\pm 5\%$.

V&V for higher statistical moments and a full pdf is still an open research question, but partial results have been obtained. Convergence properties of the second moments of concentration and the CDF (cumulative distribution function) for a RT instability are analyzed in [13, 15, 22]. Convergence of the CDFs for the joint concentration-temperature (micro) variables of an RM instability were studied in [27, 28]

The primary comparison issues addressed in this paper is the comparison of FT/LES/SGS to ILES and to DNS, as well as FT compared to DNS.

A separate question is the comparison of the variety of turbulence algorithms which do include explicit SGS terms. The reader is referred to survey and review documents e.g., [30, 18] for this active research topic. We also mention the approximate deconvolution method (ADM) [39].

### 7.2. A new V&V study

Practical engineering calculations depend on RANS simulations, in which only the large scale, problem specific scales are resolved, while none of the turbulent scales are resolved. This method requires extensive modeling, and generally extensive data to set model parameters in a problem specific manner. As experimental data is expensive or otherwise not always available, LES or DNS are often used to fill in the missing data. For this purpose second moments of the solution primitive variables are needed, as these are the quantities modeled by RANS, and for which parameters are required.

We find new issues not encountered in the V&V studies referenced in Tables 1 and 2, which concentrated on MZ width. In many respects, the convergence of mean solution quantities follows that of the MZ. The new issues are

1. Second moments may fail to converge in a simulation for which the MZ or mean flow quantities have converged. More generally, the required resolution for convergence to occur depends on the functional used to assess convergence and the accuracy required.
2. DNS has its own needs for V&V, in that judgements are involved in assessing the DNS criteria of "full resolution of all relevant quantities".
3. Near DNS simulations studied here are shown not to require LES/SGS terms, but may still contain transport related numerical artifacts affecting the numerical and thus the total $Sc$ and $Pr$. The RNG analysis contributes to understanding the possibility of numerically generated SGS terms.

We study the flow of hot and cold water over two horizontal channels, starting at a splitter plate and entering an observational chamber [31]. The flow is noisy with initial perturbations measured and used in the simulations. A normalized mixture-velocity correlation $\theta$ and two second velocity moments were recorded. Simulations using the 10th order accurate compact stencil central difference code Miranda were conducted at a nearly DNS level, meaning that the mesh was 2× finer than the Kolmogorov scale and 1.2× coarser than the Batchelor scale [31]. All simulations were based on in-

compressible codes, so that the hot and cold water were treated as distinct miscible fluids with a Schmidt number $Sc = 7$. The Miranda simulation and experimental data are compared to a converged series of FT/LES/SGS simulations.

The velocity-concentration correlations show the converged FT/LES/SGS simulation going through all but a few possibly anomalous experimental data intervals, while the Miranda simulation missed all of the late time experimental data by 10 to 30%; Error bars attributed to the data analysis of the Miranda simulation improve on this comparison.

The flow is marginally turbulent, and could be better characterized as stirring rather than turbulent mixing. For this reason the SGS terms played no role in the FT/LES/SGS simulation; virtually identical results were obtained with and without their use. In this case the simulation could be called FT/ILES. The resolution was two, four, eight times coarser than that used in the Miranda simulation, and was truely LES, i.e., not close to DNS. As indicated in Table 2, the two codes agree with the experiments for the value of $\alpha$. See Figure 1 for the velocity-concentration 2nd moment code comparison and validation study. This study indicates an improved performance of FT/LES/SGS relative to Miranda in regard to agreement to experimental data. Results for the two velocity correlations were inconclusive, with all three data (experiment and two simulations studies) in qualitative agreement but lacking detailed agreement among any two of the three. See Figure 2.

In Table 3 we summarize the conclusions of multiple V&V and code comparison studies. We indicate separately the importance of the full FT/LES/SGS algorithm and of each of its FT and LES/SGS portions, regarding the MZ, the cut cell thermodynamics and second moments of single point statistics (2nd Moments). Convergence of means of the solution primitive variables generally follows the convergence of the MZ, and is not considered separately. The table entry U indicates unknown and the entry N indicates that neither FT nor LES/SGS appear to be important. The table entries concern fluids only. FT would appear to have a value regarding cut cell variation in strength and opacity, an issue not studied. Plasmas generally have small $Sc$ and $Pr$ numbers and will follow the fluids case only for $Sc \geq 0.3$ or $Pr \geq 0.3$, based on estimates of numerical diffusion for typical Eulerian codes. Estimates of the $Pr$ and $Sc$ values that arise in an inertial confinement implosion, an example of a plasma flow, are given in [35].

### 7.3. FTI: the Front Tracking API

As the improvement of the FronTier simulations over the Miranda code lies in its use of Front Tracking, we explain the design of this software pack-

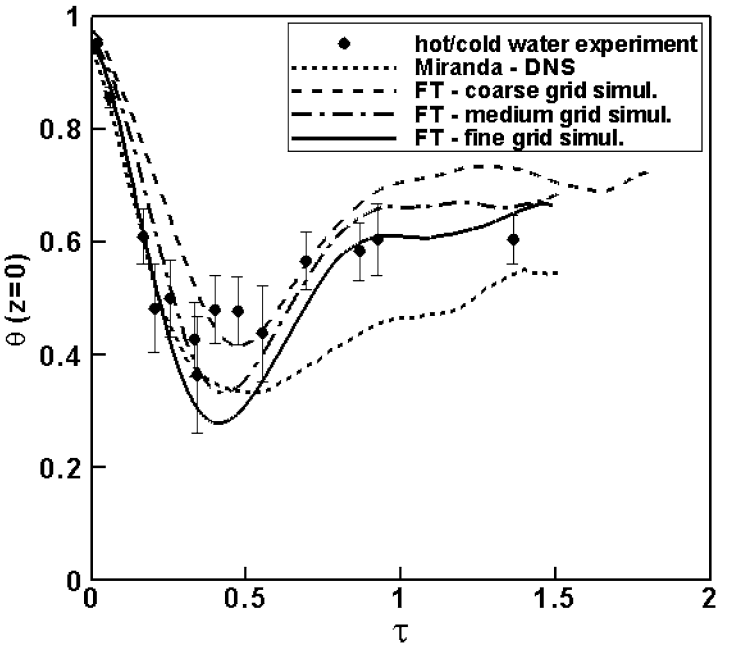


Figure 1: A nearly DNS Miranda simulation of flow of hot and cold water over a splitter plate and into an observational channel, giving rise to a Rayleigh-Taylor mixing flow. Plotted is the mixing coefficient $\theta(\tau) = \langle f(1-f)\rangle / \langle f\rangle \langle 1-f\rangle$ on the center plane of the MZ as a function of the dimensionless time $\tau$ [31], where $f$ is the mixing fraction (of hot vs. cold water). In addition, three FronTier simulations of this same experiment are plotted with two, four and eight times coarser grid resolutions.

age. A front is a triangulated surface, moving dynamically in a flow. Front Tracking, at its essence, is a software package to manage the dynamics of this surface and its interaction with a physics (client) code. To separate these two roles, to allow ease of use by a client code, and to separate the surface management issues from the user, we have introduced an application programming interface (API) called FTI.

The main client functions required to use FTI are to propagate a front point and to form a modified stencil for finite difference stencils that cross the front. Both depend on front points, which are two sided (double valued) states located at front points. These are not true dynamic variables, but are computed on the fly from the interior (regular grid cell) states. To compute a front point, a one-sided interpolation/extrapolation algorithm is needed,

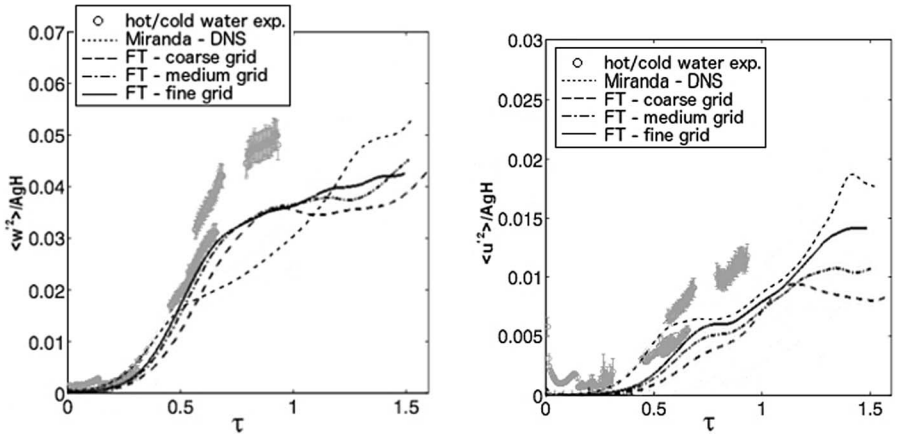


Figure 2: Velocity second moments, comparing experiment to the Miranda and sequence of FT/LES/SGS simulations Left[1]: $\langle v_z' v_z' \rangle$; right: $\langle v_x' v_x' \rangle$. Note the difference of scales in the two plots, so that the vertical correlation (left) accounts for approximately 80% of the TKE. While the converged FT/LES/SGS simulations show an advantage over Miranda in comparison to experiment, our main conclusion is that no two of the three data sets (two simulation codes and one experiment) show satisfactory agreement, indicating that further studies, including new experiments, are needed.

which determines extrapolation of interior states to the front using values from a single side of the front. The resulting pair of states are called the outer front states, and they define a Riemann problem, to be solved in the direction normal to the front. The midstates of this Riemann problem are the front states.

The conservative version of FTI (not yet implemented) is described in [16]. FTI has been installed in the High Energy Density Code FLASH, and it should be noted that the installation consumed about two weeks of effort, with another two weeks for debugging and testing.

The primary benefit of FTI is to reduce numerical diffusion associated with steep gradients or discontinuities. Thus its value decreases as the simulation progresses and the gradients become less pronounced. On the other hand, the cost and complexity of the fronts increase with time. Thus, there is a benefit in the selective untracking of portions of the front in late time. We regard FTI as the ultimate ALE (Arbitrary Eulerian Lagrangian) code, in the sense that the Lagrangian aspect of the code is confined to a surface. As

[1]Corrects error in [11].

Table 3: The role of Front Tracking (FT) and LES with subgrid models (LES/SGS) for the modeling or three solution details (mixing zone edges, cut cell thermodynamics and second moments of the solution state variables) for several cases of RT and RT instabilities. The entry FT/LES/SGS or FT indicates the code feature of importance for the indicated problem. The entry N indicates neither FT nor SGS/LES appear to be important, while U indicates an unknown case

| | MZ Edge | Cut Cell Thermodynamics | 2nd Moments |
|---|---|---|---|
| RT (fluids) | | | |
| High $Re$ | FT/LES/SGS [20, 9, 4] | U | U |
| Low $Re$ | N [31]; this work | U | FT (this work) |
| RM (fluids) | N [25] | FT [25] | U |

with all ALE codes, in late time there is a need to convert progressively to an Eulerian mode. FTI is no exception to this rule, but by design, the Eulerian conversion can be postponed to far later times that is possible with ALE in general. Selective untracking is among our future plans and the reported simulation did not use the feature.

## 8. Discussion

We have re-examined the relation between LES and the RNG. LES cannot be an RNG fixed point as it fails to be scale invariant. However, the RNG expansion still applies, and based on this, we derive a closed form expansion for the unclosed SGS terms. To leading order, this expansion coincides with the Leonard stress in the derivation of the dynamic SGS models. The full expansion of the unclosed terms suggests a higher order determination of the model coefficients. For design of aircraft and for flow in pipes, lift and drag, the important observables, are macro in nature. For reactive flows, such as combustion, micro observables of atomic mixing properties are fundamental. They are the direct input to continuum level chemical reaction rate laws. Accurate modeling of micro observables allows finite rate LES chemistry and elimination of flame structure models from combustion simulations. Practical requirements of engineering simulations also lead to the importance of LES and of compressible simulations.

We discuss the possible role of numerical and physical modeling issues in the selection of a high Re limit point. We have identified the RNG relevant variables as the dimensionless parameters of the Euler equation. The identification of these parameters as relevant is conventional within RNG

methods, but it is neither demonstrated by the results of this paper nor is it essential to them. RNG theories may also include dimensional equation parameters, as with the mass of the electron in quantum field theory. Some of the dimensionless turbulent transport parameters could turn out to be irrelevant (decreasing more rapidly under RNG iterations) and still parameterize non-unique solutions, to be achieved by a stronger fractal or numerical algorithmic forcing.

The scientific understanding of turbulent mixing and its dependence on Re in the simple "pure hydro" example considered here provides an indispensable foundation for the study of mixing in the multi-physics context likely to prevail in complex problems of engineering interest.

## Acknowledgements

This research was supported in part by the U.S. Department of Energy via Los Alamos National Laboratory contract number 228022, Stanford University contract number 60541887107908 and the Army Research Organization grant numbers W911NF1310249 and W911NF1410482. This research used resources of the National Energy Research Scientific Computing Center, a DOE Office of Science User Facility supported by the Office of Science of the U.S. Department of Energy under Contract No. DE-AC02-05CH11231. Los Alamos National Laboratory Preprint Number LA-UR-12-26149. Stony Brook University Preprint Number SUNYSB-AMS-15-05.

## References

[1] B. Camguilhem, A. Honein and P. Moin, Evaluation of a monotone integrated large eddy simulation algorithm. *American Physical Society, Division of Fluid Dymanics 55th Annual Meeting* (Nov. 2002), abstract JK.005.

[2] G.-Q. Chen and J. Glimm, Kolmogorov's theory of turbulence and inviscid limit of the Navier-Stokes equations in $R^3$. *Commun. Math. Phys.* **310** (2012), 267–283. MR2885620

[3] R. A. Clark, J. H. Ferziger, and W. C. Reynolds, Evaluation of subgrid-scale models using an accurately simulated turbulent flow. *J. Fluid Mech.* **91** (1979), 1–16.

[4] G. Dimonte, D. L. Youngs, A. Dimits, S. Weber, M. Marinak, S. Wunsch, C. Garsi, A. Robinson, M. Andrews, P. Ramaprabhu, A. C. Calder,

B. Fryxell, J. Bielle, L. Dursi, P. MacNiece, K. Olson, P. Ricker, R. Rosner, F. Timmes, H. Tubo, Y.-N. Young, and M. Zingale, A comparative study of the turbulent Rayleigh-Taylor instability using high-resolution three-dimensional numerical simulations: The Alpha-Group collaboration. *Phys. Fluids* **16** (2004), 1668–1693.

[5] G. Eyink and N. Goldenfeld, Analogies between scaling in turbulence, field theory, and critical phenomena. *Phys. Rev. E* **50** (1994), 4679–4683. MR1385424

[6] E. Garnier, M. Mossi, P. Sagaut, P. Comte, and M. Delville, On the use of shock-capturing schemes for large-eddy simulation. *J. Comput. Phys.* **153** (1999), 273.

[7] E. George, J. Glimm, X.-L. Li, Y.-H. Li, and X.-F. Liu, Influence of scale-breaking phenomena on turbulent mixing rates. *Phys. Rev. E* **73** (2006), 016304. MR2223067

[8] M. Germano, Turbulence: The filtering approach. *J. Fluid Mech.* **238** (1992), 325–336. MR1166088

[9] J. Glimm, D. H. Sharp, T. Kaman, and H. Lim, New directions for Rayleigh-Taylor mixing. *Phil. Trans. R. Soc. A* **371** (2013), 20120183. MR3123296

[10] A. Honein and P. Moin, Numerical aspects of compressible turbulence simulations. *Report No. TF-92, Stanford Univ.* (2005).

[11] Wenlin Hu, Statistical moments in variable-density incompressible mixing flows. *PhD thesis, Stony Brook University* (2015). MR3438977

[12] K. Kadau, T. C. Germann, N. G. Hadjiconstantinou, P. S. Lomdahl, G. Dimonte, B. L. Holian, and B. J. Alder, Nanohydrodynamics simulations: An atomistic view of the Rayleigh-Taylor instability. *Proc. Natl. Acad. Sci.* **101** (2004), 5851–5855. MR2048456

[13] T. Kaman, R. Kaufman, J. Glimm, and D. H. Sharp, Uncertainty quantification for turbulent mixing flows: Rayleigh-Taylor instability. *Uncertainty Quantification in Scientific Computing* **377** of the series IFIP Advances in Information and Communication Technology, Springer (2012), 212–225.

[14] T. Kaman, H. Lim, Y. Yu, D. Wang, Y. Hu, J.-D. Kim, Y. Li, L. Wu, J. Glimm, X. Jiao, X.-L. Li, and R. Samulyak, A numerical method for the simulation of turbulent mixing and its basis in mathematical theory. *Lecture Notes on Numerical Methods for Hyperbolic Equations:*

*Theory and Applications: Short Course Book, CRC/Balkema, London* (2011), 105–129. MR2867600

[15] Ryan Kaufman, Tulin Kaman, Yan Yu, and James Glimm, Stochastic convergence and the software tool W*. *Numerical Methods for Hyperbolic Equations, CRC, Taylor and Francis Group, London* (2012), 37–41. MR3290176

[16] R. Kaufman, H. Lim, and J. Glimm, Conservative front tracking: The algorithm, the rationale and the API. *Bulletin of the Institute of Mathematics, Academia Sinica New Series* (2015).

[17] A. N. Kolmogorov, The local structure of turbulence in incompressible viscous fluid for very large Reynolds' numbers. *Doklady Akad. Nauk. SSSR* **30** (1941), 301–305. MR0004146

[18] Eric Lamballais, Rainer Friedrich, Bernard J. Geurts, and Olivier Metais, Direct and Large Eddy Simulation VI. *Springer Verlag, Heidelberg* (2006).

[19] A. Leonard, Energy cascade in large-eddy simulations of turbulent fluid flows. *Adv. Geophys. A* **18** (1974), 237–248.

[20] H. Lim, J. Iwerks, J. Glimm, and D. H. Sharp, Nonideal Rayleigh-Taylor mixing. *Proc. Nat. Acad. Sci.* **107** (2010), 12786–12792. MR2670988

[21] H. Lim, J. Iwerks, Y. Yu, J. Glimm, and D. H. Sharp, Verification and validation of a method for the simulation of turbulent mixing. *Physica Scripta* **T142** (2010), 014014.

[22] H. Lim, T. Kaman, Y. Yu, V. Mahadeo, Y. Xu, H. Zhang, J. Glimm, S. Dutta, D. H. Sharp, and B. Plohr, A mathematical theory for LES convergence. *Acta Mathematica Scientia* **32** (2012), 237–258. MR2921875

[23] X.-F. Liu, E. George, W. Bo, and J. Glimm, Turbulent mixing with physical mass diffusion. *Phys. Rev. E* **73** (2006), 056301. MR2242603

[24] T. Ma, Large-eddy simulation of variable density flows. *PhD thesis, University of Maryland* (2006).

[25] T. O. Masser, The effects of temperature equilibrium in mixed cell hydrodynamics. *PhD thesis, Stony Brook University* (2007). MR2712285

[26] W. D. McComb, Renormalization Methods. *Oxford University Press, Oxford* (2004). MR2038105

[27] J. Melvin, P. Rao, R. Kaufman, H. Lim, Y. Yu, J. Glimm, and D. H. Sharp, Atomic scale mixing for inertial confinement fusion associated hydro instabilities. *High Energy Density Physics* **9** (2013), 288–298.

[28] J. Melvin, P. Rao, R. Kaufman, H. Lim, Y.Yu, J. Glimm, and D. H. Sharp, Turbulent transport at high reynolds numbers in an ICF context. *J. Fluids Eng.* **136** (2014), 091206.

[29] P. Moin, K. Squires, W. Cabot, and S. Lee, A dynamic subgrid-scale model for compressible turbulence and scalar transport. *Phys. Fluids A* **3** (1991), 2746–2757.

[30] C. Montveau and J. Katz, Scale-invariance and turbulence models for large-eddy simulation. *Ann Rev. Fluid Mech.* **32** (2000), 1–32. MR1744302

[31] N. Mueschke and O. Schilling, Investigation of Rayleigh-Taylor turbulence and mixing using direct numerical simulation with experimentally measured initial conditions. I. Comparison to experimental data. *Phys. Fluids* **21** (2009), 014106.

[32] Nicholas J. Mueschke, Experimental and numerical study of molecular mixing dynamics in Rayleigh-Taylor unstable flows. *PhD thesis, Texas A and M University* (2008).

[33] A. S. Neto, D. Grand, O. Métais, and M. Lesieur, A numerical investigation of the coherent vortices in turbulence behind a backward-facing step. *J. Fluid Mech.* **256** (1993), 1–25.

[34] P. Ramaprabhu and M. Andrews, Experimental investigation of Rayleigh-Taylor mixing at small atwood numbers. *J. Fluid Mech.* **502** (2004), 233–271.

[35] V. Rana, *PhD thesis, Stony Brook University*, In preparation.

[36] K. I. Read, Experimental investigation of turbulent mixing by Rayleigh-Taylor instability. *Physica D* **12** (1984), 45–58.

[37] V. Scheffer, An inviscid flow with compact support in space-time. *J. Geom. Anal.* **3** (1993), 343–401. MR1231007

[38] V. S. Smeeton and D. L. Youngs, Experimental investigation of turbulent mixing by Rayleigh-Taylor instability (part 3). *AWE Report Number 0 35/87* (1987).

[39] S. Stolz and N. A. Adams, An approximate deconvolution procedure for large-eddy simulation. *Phys. Fluids* **11** (1999), 1699–1701.

[40] S. Sukoriansky, B. Galperin, and I. Staroselsky, Cross-term and $\epsilon$-expansion in RNG theory of turbulence. *Fluid Dynamics Research* **33** (2003), 319–331. MR2012615

[41] V. Yakhot and S. A. Orszag, Renormalization group analysis of turbulence. *Phys. Rev. Lett.* **57** (1986), 1722–1724. MR0934343

[42] V. Yakhot and S. A. Orszag, Renormalization group analysis of turbulence I: Basic theory. *J. Sci. Comput.* **1** (1986), 3–51. MR0870313

James Glimm
Department of Applied Mathematics and Statistics
Stony Brook University
Stony Brook, NY 11794-3600
USA
*E-mail address:* glimm@ams.sunysb.edu

Bradley J. Plohr
Theoretical Division
Los Alamos National Laboratory
Los Alamos, NM 87545
USA
*E-mail address:* plohr@lanl.gov

Hyunkyung Lim
Department of Applied Mathematics and Statistics
Stony Brook University
Stony Brook, NY 11794-3600
USA
*E-mail address:* hyulim@ams.sunysb.edu

Wenlin Hu
Department of Applied Mathematics and Statistics
Stony Brook University
Stony Brook, NY 11794-3600
USA
*E-mail address:* whu@ams.sunysb.edu

David H. Sharp
Theoretical Division
Los Alamos National Laboratory
Los Alamos, NM 87545
USA
*E-mail address:* dcso@lanl.gov

Received November 23, 2015